EUROPEAN FUSION DEVELOPMENT AGREEMENT

EFDA–JET–PR(05)04

P. Arena, L. Fortuna, M. Bruno, G. Vagliasindi, A. Murari, P. Andrew,
G. Mazzitelli, and JET EFDA contributors

Cellular Nonlinear Networks for Strike-Points Localization at JET

Cellular Nonlinear Networks for Strike-Points Localization at JET

P. Arena[1], L. Fortuna[1], M. Bruno[1], G. Vagliasindi[1], A. Murari[2], P. Andrew[4], G. Mazzitelli[4] and JET EFDA contributors*

[1]Dipartimento di Ingegneria Elettrica, Elettronica e dei Sistemi, Università di Catania, v.le A. Doria 6, I-95125, Catania, Italy
[2]Consorzio RFX – Associazione EURATOM ENEA per la Fusione, Corso Stati Uniti 4, I-35127, Padua, Italy
[3]EURATOM/UKAEA Fusion Assoc., Culham Science Centre, Abingdon, Oxon, OX14 3DB, UK
[4]Associazione Euratom-ENEA sulla Fusione, C.R. Frascati - C.P. 65, I-00044 Frascati (Roma) Italy
** See annex of J. Pamela et al, "Overview of JET Results ", (Proc.20 th IAEA Fusion Energy Conference, Vilamoura, Portugal (2004).*

Preprint of Paper to be submitted for publication in
Review of Scientific Instruments

ABSTRACT.
At JET the potential of fast image processing for real time purposes is actively investigated. Particular attention is devoted to smart sensors based on System on Chip Technology. In detail, to support and complement the magnetic diagnostics in the real time localization of the strike point position in the divertor, the data of the infrared cameras were processed with a new chip implementing a Cellular Nonlinear Network (CNN) structure. This circuit consists of two layers of CMOS components, the first being the sensor and the second implementing the actual CNN. With this innovative hardware, it has been possible to determine the position of maximum thermal load with time resolution of the order of 30 ms. Good agreement is found with the resuls of the thermocouples in the divertor, proving the potential of the infrared data to locate the region of maximum thermal load. The results are also confirmed by JET magnetic codes, both those used for the equilibrium reconstructions and those devoted to the identification of the plasma boundary.

I. INTRODUCTION AND OVERVIEW

Real time control is a rapidly expanding subject also in the field of Nuclear Fusion. In ITER, and even more in the reactor, the number of quantities to be controlled in feedback will be much higher than in present day machines, given the complexity of the device and the safety issues involved. On the other hand, the operating environment of the next generation experiments is going to pose severe problems to the diagnostics and, as a consequence, to the real time schemes. The high neutron fluence and steady state operation are two of the major issues of concern in this perspective. These conditions are expected to affect some of the most fundamental measurements in a Tokamak device, the magnetic diagnostics, and can therefore potentially create serious difficulties to the most basic control systems. In fact, in present day machines the magnetic measurements rely on the established technology of pick-up coils, which, being based on the flux variation, have intrinsic problems in coping with long steady state fields. Moreover, high neutron fluence is known to cause several problems to cables, including the generation of common mode currents, which can produce dangerous drifts in the acquired signals. Since, in order to avoid the shielding due to the passive conductors, the coils have to be located near the plasma this neutron induced damage is certainly a serious issue for the Next Step. Several alternatives are therefore being assessed within the community to complement the pick-up coil measurements with other diagnostics to obtain a more reliable identification of the plasma boundary in ITER. The use of reflectometric data and radiation hard Hall probes are two of the main alternatives presently under investigation. A complementary approach consists of using the visual information derived from infrared and/or visible cameras. In this paper the first results obtained with the new technology of Cellular Networks (CNN) for image processing are reported.

Since the main mission of JET consists in developing integrated scenarios for ITER, in the last years a lot of efforts have been devoted to the development of innovative real time tools [1, 2]. Particular attention was devoted to the magnetic measurements, since the requirements of discharges

with higher elongation and shape, necessary to improve plasma performance, pose severe demands on the control of the equilibrium. In general the real time reconstruction of the plasma boundary is necessary for plasma control, disruption avoidance and heat load protection. In particular, the accurate localization of the strike points on the divertor plates is imperative to estimate the power load on the carbon tiles, the recycling properties of the configuration, and in general to assess the safety features of the pulse. To this end, the magnetic reconstruction of the separatrix done by the XLOC code [3] has proved to be fairly accurate and quite robust during many years of operation and offline extensive validation. On the other hand, even if long pulses do not seem to constitute a particular threat in the case of JET, it has already been experienced in several occasions that magnetic data can suffer from non-contemplated deviations due to eddy currents during fast transient events. In particular, the divertor is lodged in a massive conducting structure under which the diagnostic sensors measuring the magnetic field are positioned: when for example the divertor coils command the sweeping of the strike points, the reconstruction of their positions based on these measurements can become particularly critical. Moreover, whereas the strike points are mainly defined by the position of the intersection between the separatrix and the divertor plates, the power deposition involves a larger areas and depends on the flux expansion of the magnetic field lines. The fine structure of the thermal load in the divertor is therefore not univocally and simply linked to the position of the separatrix.

In this perspective visual information, from suitable cameras, can be in principle very useful to verify and complement the magnetic reconstruction of the plasma boundary, providing additional details on the location of the strike points and the power deposition. On the other hand, manipulating images in a feedback loop with the necessary time resolution can be problematic since the amount of data to be processed is very high. To solve this problem, the approach of CNNs was adopted (see Section 2), since it is particularly suited to fast computation. The CNNs are array of simple, identical, locally interconnected nonlinear dynamics circuits called cells [4]. Each cell interacts, via weighted connections, with the cells in the neighbourhood of a limited radius. The analog implementation permits a parallel way of processing: in fact the exchange of information among cells occurs in extremely short times, represented by the time constant of the single cell. This characteristic of the CNN approach is essential in the case of image processing in real time. The chip implementing the CNN and used to obtain the results reported in this paper is the ACE16K, designed by the IMSE-CNM under the European Commission Funded DICTAM project [5]. It consists of two layers of CMOS components. The first is the actual sensor whereas the second comprises the architecture necessary to implement the CNN. This innovative System on Chip (SoC) technology was used to process the images of JET infrared cameras (Section 3), using a particular procedure explicitly developed for this application (see Section 4). The positive results obtained in the determination of the strike points are shown in Section 5, where a systematic comparison with the estimate of XLOC and the divertor thermocouples is also reported. The remaining issues and the lines of future works are discussed in the final Section

2. CELLULAR NEURAL NETWORKS FOR IMAGING APPLICATIONS

The CNN was introduced by L.O. Chua [4,6] in 1988 to be employed in such areas as image processing and pattern recognition. The architecture of the CNN is constituted of a basic circuit called cell, containing linear and nonlinear circuit elements (see Fig.1).

Each cell in a CNN is connected to its local neighbouring cells, so a direct interaction occurs only among adjacent cells. An example of a two-dimensional CNN is shown in Fig.2.

The neighbourhood of cell on the i-th row and j-th column, denoted by C(i, j), has the following definition:

$$N_r(i, j) = \{C(k, l) \,|\max\{\{|k - l|, |l - j|\} \le r, \} \\ 1 \le k \ge M; \quad 1 \le l \ge N; \tag{1}$$

where r is a positive integer number, which fixes the dimension of the neighbourhood.

A CNN is entirely characterized by a set of nonlinear differential equations associated with the cells in the circuit. The mathematical model for the state equation of the single cell, also called Full Signal Range (FSR), as implemented in the CNN Universal chip family [7], is given by the following set of relations:

$$C_x \frac{dx_{ij}(t)}{dt} = -\frac{1}{R_x} g\left(x_{ij}(t)\right) + \sum_{C(k,l) \in N_r(i,j)} A(i, j; k, l)\, y_{kl} + \sum_{C(k,l) \in N_r(i,j)} B(i, j; k, l)\, u_{kl}(t) + I \tag{2}$$

and the output equation is:

$$y_{ij}(t) = y_{ij}(t) \tag{3}$$

where:

u, x, and y denote the input, state, and output of the cell, respectively; R_x and C_x are the values of the linear resistor and linear capacitor, that determine the time constant of the circuit; A(i, j; k, l) and B(i, j; k, l) are the feedback and control templates respectively; I is the bias term, that is constant for all the CNN cells; g(x) is the nonlinear function in the state equation (2), depicted in Fig.3. The templates are matrixes that contribute to implement the analysis algorithm (see later).

This last element is the main difference between the classical Chua-Yang CNN model [4] and the FSR model. In fact, in the former one, the nonlinearity enters into the output equation and is the integral of g(x). In Espejo et al. [7] it has been demonstrated that the two mathematical models are equivalent.

As previously reported, one of the main applications of CNNs is image processing [8, 9]. In this case the input image is mapped on the CNN in such a way that each image pixel is 6 associated to the input or initial state of a particular cell. The CNN evolution implies a transformation of the input image into the corresponding output image obtained directly by the equation (2). In this contest, the template operators work like the instructions in a programming code. Even if a direct

procedure to derive the template values according to the particular task has not been derived yet, a huge amount of templates and template algorithms is already available in literature [10].

The hardware prototype system used in this application is based on two fundamental parts: the CNN Universal Chip prototype, which is a 128×128 CNN chip [11], and the CNN Chip Prototyping and Development System (CCPS) platform designed in Budapest [12]. The chip is a new generation 128×128 Focal-Plane Analog Programmable Array Processor (FPAPAP), manufactured in a 0.35μm standard digital 1P-5M CMOS Technology. It contains close to four millions transistors, 80% of them working in analog mode, and exhibits a relatively low power consumption (<4W, i.e. less than 1μW per transistor). Computing vs. power peak values are in the order of 1TeraOPS/W, while maintained VGA (640x480) processing throughputs of 100Frames/s are possible with about 10-20 basic image processing tasks on each frame. The architecture of the system is sketched in Fig.4.

ACE16K can be basically described as an array of 128×128 identical, locally interacting, analog processing units designed for high speed image processing tasks requiring moderate accuracy (around 8bits). The system contains a set of on-chip peripheral circuitries that, on one hand, allow a completely digital interface with the host, and on the other provide high algorithmic capability by means of conventional programming memories where the algorithms are stored.

Although ACE16K is essentially an analog processor (computation is carried out in the analog domain), it can be operated in a fully digital environment. For this purpose, the prototype incorporates a bank of Digital-to-Analog (for input) and Analog-to-Digital (for output) converters at the images I/O port. ACE16K is conceived to be used in two alternative 7 ways. First, in applications where the images to be processed are directly acquired by the optical input module of the chip, and second, as a conventional image co-processor working in parallel with a digital hosting system that provides and receives the images in electrical form. The second mode of operation is the one adopted to obtain the results presented in this paper.

The chip can be divided into five functional blocks. First, the analog processing core, which comprises the inner array of 128×128 identical cells, a ring of border cells used to establish spatial boundary conditions for image processing, and several buffers driving analog and digital signals to the cell array. Second, the programming block, which contains two 64×32 SRAM digital memories used to store the algorithms to be executed by the chip, six 32×32 SRAM digital memories used to store, in 8bits format, different sets of the analog coefficients controlling the cell-to-cell interactions, some global bias signals, and some references used by the optical input module (precharging values, etc.). The programming memory contains also all the circuitry needed for external accesses to these memory blocks, and to transmit the programmed values to the analog processing core. This includes digital buffers for digital instructions, and digital-to-analog converters and analog buffers for weights (cell-to-cell interactions) and references. The remaining blocks are dedicated to images I/O tasks. The global I/O control unit generates the signals required for I/O image accesses. This includes row and column addressing signals (automatically generated in a sequential way), and control of the Digital-to-Analog and Analog-to-Digital I/O converters bank.

The chip uses a 32 bits bidirectional data bus, for external communication, and several address buses for the different blocks within the programming memory. The external interface follows very simple hand-shaking protocols. Table I summarizes the main characteristics of the prototype.8

3. JET DIVERTOR AND THE DIAGNOSTICS FOR THE DETERMINATION OF THE STRIKE POINTS.

In Tokamak plasmas, the divertor is the region of the vacuum vessel explicitly designed to handle the power losses. In JET history several topological solutions were tested for the divertor. The one used for the discharges, whose results are described in this paper, is shown schematically in Fig.5. The typical X-point plasma configuration is also shown: it is characterized by the existence of a separatrix, and a scrape-off layer. The first one is the last closed flux surface that separates the closed magnetic field lines from the open ones that intersect the vacuum vessel, while the scrape-off layer is the region of the plasma where the magnetic field lines intersect wall elements, in this case the divertor. The plasma power losses are deposited along this region. The intersection of the separatrix with the divertor target plate represents a strike point.

In JET the position of the strike points is mainly derived from the magnetic measurements. They consist of various loop and pick-up coils located around the vacuum vessel. These measurements, performed at some distance from the plasma, can be extrapolated across the current-free region to identify the last closed flux surface. The code used at JET to determine the plasma shape and therefore also the position of the strike points is XLOC. The main output of XLOC consists of determining the last closed flux surface, also called the separatrix.

In JET divertor various thermocouples are also located in the divertor tiles, covering the whole region were the magnetic field lines can intersect material surfaces. From the thermocouple signals it is possible to identify the region of maximum thermal load which can be assimilated to the position of the strike points.

Infrared imaging is another very useful diagnostic to derive information about the power deposition in JET divertor. Nowadays two cameras are available at JET. They measure the infrared radiation in the interval 3-5μm with a resolution of 128×128 pixels. The views of the 9 cameras are reported in Fig.6. One camera sees the outer leg of the divertor, the other the inner leg and, as far as real time control is concerned, the two views can be considered representative of the entire divertor, given the toroidal symmetry of the machine.

The first analysis of the infrared emission consisted of determining how the presence of the Strike-Points reflects itself in the visual features of the camera images. In Fig.7 an image captured by the infrared camera is shown. As already mentioned, the strike points represent the region of maximum thermal load on the divertor region. Therefore the strike points can be assimilated to the region of maximum brightness in an infrared image. A first manual analysis of JET IR cameras proved that the shape of the strike points consists of two thin bands of high emission in the whole divertor region, oriented in the toroidal direction. These last two visual features obviously depend

on the position and tilt of the camera, but they can be considered invariant in this application, as the camera is installed with a fixed position and orientation.

The second preliminary analysis step was dedicated to the camera calibration, which, in the context of three-dimensional vision, is the process of determining the internal camera geometric and optical characteristics (intrinsic parameters) and the 3-D position and orientation of the camera frame relative to a certain world coordinate system (extrinsic parameters). Extrinsic parameters are needed to transform object coordinates to a camera centered coordinate frame. The pinhole camera model adopted is based on the principle of collinearity, where each point in the object space is projected by a straight line through the projection center into the image plane. The main problem is the perspective projection, which in general is not a shape preserving transformation. Only lines are mapped as lines on the image plane. Two- and three-dimensional objects with a non-zero projection area are distorted if they are not coplanar with the image plane. The aforementioned problems were solved using a dedicated 3D graphic software.

In the CNN algorithms described in the following, the geometry of the divertor was used as input together with the co-ordinates in physical space and the geometrical properties 10 of the cameras. The mapping of the pixels onto the physical space of the divertor is therefore a consolidated input which is used to determine the real position of the strike points once determined their position in the image acquired by the camera.

4. THE ALGORITHM FOR THE REAL TIME IDENTIFICATION OF THE STRIKEPOINTS

A specific procedure was developed to derive the position of the strike points from the data of the infrared cameras exploiting the capabilities of CNN technology. A flowchart of the developed algorithm is depicted in Fig.8.

The algorithm has been applied on a frame extracted from the movie. This frame is the composition of the two images framing respectively the inner and the outer side of the divertor region (Fig.6 and 7). These images should have really different brightness according to the different temperature the strike points reach in the two regions of the divertor. So it is necessary to perform an independent processing.

The first operation, after loading the image from the hard disk, is an INVERSION to obtain the negative frames. This is necessary since the CNN-UM works with a grey scale that is inverted with respect to the usual image processing software. Subsequently, a THRESHOLD template is applied to the image, to identify the pixels whose value is higher than a predefined level. The result of this first processing phase is a binary image, where the black pixels represent those exceeding a given brightness threshold. In order to perform the independent processing of the two strike points, at this stage an AND operation with a mask is executed to select the pixels representing the inner (outer) strike points. To have a number of maxima useful to perform the identification of the strike points position, the number of pixels in the image is evaluated. If it is less than a given number K, the

threshold value in the THRESHOLD template is decreased by a constant value ‘j’, and the cycle is repeated.

Otherwise the LOOP stops when the K value is reached. In the algorithm implemented the K value is 50 pixels and the threshold constant decrement is set to 10.

At this stage the images of the strike points consist of a band of black pixels, corresponding to the region of maximum brightness in the divertor legs. Subsequently, a SKELETONIZATION template is applied to find the skeleton of the black-and-white bands. The algorithm comprises up to 8 templates, which should be applied circularly, always feeding the output back to the input before using the next template (see Fig.8). Once obtained the skeleton of the inner strike points the algorithm is executed a second time, starting from the inverted image, to extract the outer strike point position. Finally the results of the algorithm are stored in two picture files in the local hard drive. The various steps of the described procedure are illustrated graphically in Fig.9.

With the described approach the position of the strike points, both the inner and the outer one, can be obtained, starting from the frame loading, within 30ms. In particular the on board operations, i.e. the instructions included in the broken lined square in Fig.8, are executed in a time comprised among 13 and 19ms, depending on the brightness condition of the starting frame. The loading and downloading of the file from the hard drive takes the remainder 11ms. This last time can be definitely improved using more performing hardware to host the Aladdin Platform. This is already a time resolution more than acceptable for the vast majority of JET applications. It is indeed to be considered that in general the thermal effects, which can affect the tile temperature and change the infrared emission, do not change much on shorter time scales.

5. EXPERIMENTAL RESULTS

In order to assess the accuracy of the CNN estimate of the strike points position, a systematic comparison with the results of XLOC was undertaken. To this end the co-ordinates of the strike points obtained with the CNN were compared with the ones given by XLOC for the intersection of the separatrix with the divertor. Concerned to this last point, it is worth mentioning that for the detection of the intersection of the separatrix calculated with XLOC and the divertor an approximated shape of the divertor region is used which is reported in the Fig.10. The lines which represent the approximated divertor are the dashed ones.

The divertor region consists of two parts, the inner and the outer as reported in Fig.10. The intersection of the separatrix with the divertor region produce always four co-ordinates, two for the inner and two for the outer divertor region, that represent the R and Z positions (R radial, Z vertical) at which the separatrix crosses the dashed line reported in Fig.10.

In Fig.11 to 14 the comparison between results obtained with XLOC and the ones obtained with the CNN Image Processing for the inner and the outer divertor region is reported. A good agreement between the two diagnostics can be appreciated, but a clear systematic discrepancy is also evident in both the R and Z position. The discrepancy is to be ascribed to the fact that, due to the flux

expansion, in general the maximum of the power load does not always occur exactly at the position where the separatrix intersects the divertor tiles but it slightly shifted outwards. A much better agreement with the magnetic measurements was indeed found taking this effect into account. This was achieved considering the intersection with the divertor of the magnetic lines a bit outside the last closed flux surface. In particular we used two field lines 5 mm and 10mm outside the separatrix (the 5 and 10mm refer to the position of the field line as calculated at the equatorial plane). In Fig.11 to 14, the interceptions calculated for these two lines, obtained using the EFIT equilibrium code, are reported. It is possible to observe that the CNN calculated values are almost always among the XLOC separatrix and the 10 mm outside flux line, in accordance to the fact that the maximum power load, i.e. what is detected by the CNN approach, is located in a point inside the scrape-off layer.

In order to confirm that the original discrepancy was due to the shift of the point of maximum power load with respect to the intercept of the separatrix with the divertor tiles, a survey of the thermocouple signals was also performed. In Fig.15 and 16, the typical evolution in time of the strike points estimated by XLOC, the co-ordinates obtained by the CNN and the position of maximum load as given by the thermocouples are compared. In JET indeed an array of thermocouples determine the poloidal topology of the tile temperature in the divertor (see Fig.10). Even if the spatial resolution of the array is quite coarse, for the discharges in which the strike points are close to the position of one thermocouple, quite accurate information can be derived on the peak thermal load.

As shown in Fig.15 and 16, the co-ordinates of the strike points as estimated by the CNN are in accordance with the results of the thermocouples. In fact, in Fig.15 (bottom) the trend of the thermocouple suggests that the strike point is located among the location of the thermocouple 3U and 3L, as confirmed by the trend of the strike point coordinates calculated by the CNN. In Fig.16, the thermocouple trend suggests that the strike point is located first really near the position of 7U and then, after second 63, it moves to 7L. The value calculated using infrared data is in agreement with this trend: during the first phase of the shot evolution the strike position is located really near the 7U location and then it moves toward the 7L location almost at the same time when the temperature of this thermocouple rises.

To confirm the validity of our approach, a statistical comparison between the CNN estimate and the one derived from the magnetic reconstruction of the boundary was performed. In Fig. 17 the x axis shows the Z value calculated with the CNN approach, while the y axis reports the vertical interception of the flux line 5 mm outside the separatrix calculated via the EFIT software. The agreement between the two results is good: it can be noticed that the absolute error is included in the range [-1cm : +1cm] apart from some sporadic points.

DISCUSSION

As expected, the infrared emission contains a lot of useful information about the position of the strike points, allowing to study even the fine structure of the power load. Moreover, the recent

developments of CNN algorithms and the progress in SoC technology make much faster the analysis of visual data, which can be processed on time scales compatible with the real time requirements of big Tokamaks like JET. As a consequence, the proposed approach becomes quite attractive because it provides information about the maximum of the power deposition in the divertor but with high spatial and time resolution. This technique can therefore, in a certain sense, bridge the performance gap between the magnetic signals and the thermocouples. In any case, the reported results show a very good agreement with the both XLOC and the thermocouple measurements.

The described approach consists of a smart sensor obtained with CNN mathematical procedures implemented on a single chip. Together with the identification of MARFE at FTU13 this is the first use of SoC technology in the Fusion community. It is worth pointing out that similar systems, based on CMOS technology and CNN algorithms, could find other useful applications in JET, for example in the detection of the hot spots and control of the beam shine through.

In any case, in order to increase the potential of the presented approach for the identification of the strike points on the route to ITER, some improvements remain necessary. First of all the CMOS technology should be miniaturised even further to increase the speed up to about 1 ms time resolution. Moreover, in order to use the chip as a self contained detector without having to make recourse to infrared camera signals, the potential to develop a first layer sensitive to IR radiation is being investigated. Also the alternative to exploit visible radiation should not be completely dismissed a priori and further tests are planned in this direction. In the perspective of diagnosing a burning plasma, the radiation hardness of the technology should also be assessed.

ACKNOWLEDGEMENTS

The work was partially supported by the Project "Real-time visual feature extraction from plasma experiments for real time control", funded by ENEA-EURATOM, 2004

REFERENCES

[1]. A. Murari et al. accepted for publication in Plasma Physics and Controlled Fusion.

[2]. R. Felton et al., Venice, SOFT 2004

[3]. F. Sartori, A. Cenedese, F. Milani, Fusion Engineering and Design, Volumes 66-68, Part A, pp.735-739, September 2003

[4]. L. O. Chua, L. Yang, IEEE Trans. Circuits and Systems-part I, 35, pp. 1257-1290, 1988.

[5]. Dynamic Image Computing Using Tera-speed Analog Visual Processor (DICTAM) project http://www.imse.cnm.es/~dictam

[6]. L. O. Chua and T.Roska, IEEE Trans. on Circuits and Systems - part I, vol.40, pp.147-156, 1993.

[7]. S. Espejo, R. Carmona, R. Domìnguez-Castro and A. Rodrìguez-Vàzquez, International Journal of Circuit Theory and Applications, Vol. 24, pp 341-356, May-June 1996.

[8]. P. Arena, A. Basile, M. Bucolo, L. Fortuna, IEEE Trans. on Circuits and Systems - part I, vol. 50, Issue 7, July 2003, pp. 837 – 846.

[9]. P.Arena, A. Basile, L. Fortuna, J. Vandewalle, M. E. Yalcin, Int. Journal of Circuit Theory and Applications, vol. 32, no. 6, pp. 519-607, 2004.

[10]. T. Roska, L. Kek, L. Nemes, A. Zaràndy, and P. Szolgay, CNN Software Library (Template and Algorithms) Version 7.3, Hungarian Academy of sciences ed. Budapest, Hungary: Computer and Automation Institute, 1999.

[11]. A. Rodríguez-Vázquez, G. Linan-Cembrano, L. Carranza, E. Roca-Moreno, R. Carmona-Galan,F. Jimenez-Garrido, R. Dominguez-Castro, S. Espejo Meana, IEEE Transaction on Circuits and Systems-I:REGULAR PAPER, vol.51, no.5, May 2004

[12]. A. Zaràndy, T. Roska, P. Szolgay, S. Zöld, P. Földesy and I. Petràs, European Conference on Circuit Theory and Design – ECCTD'99, Design Automation Day proceedings, pp. 69-81. (ECCTD'99-DAD), Stresa, Italy, 1999.

[13]. P. Arena, A. Basile, R. De Angelis, L. Fortuna, G. Mazzitelli, S. Migliori, G. Vagliasindi, M. Zammataro, IEEE Trans. on Plasma Science, in press.

ACE16K Professional board

Operation		**Frame rate timing**
Grayscale image download	(128 × 128)	2688 frame/sec; 372μs
Grayscale image readback	(128 × 128)	3536 frame/sec; 283μs
Array operatio	(128 × 128)	9μs + N*100ns
Logical operation	(128 × 128)	3.8μs

Table 1: Technical characteristics

Operation	**Time (ms)**
Load from HD	2ms
On Board operations	13 - 19ms
Download to HD	9ms
Total	**30ms**

Table 2: Execution time of the algorithm

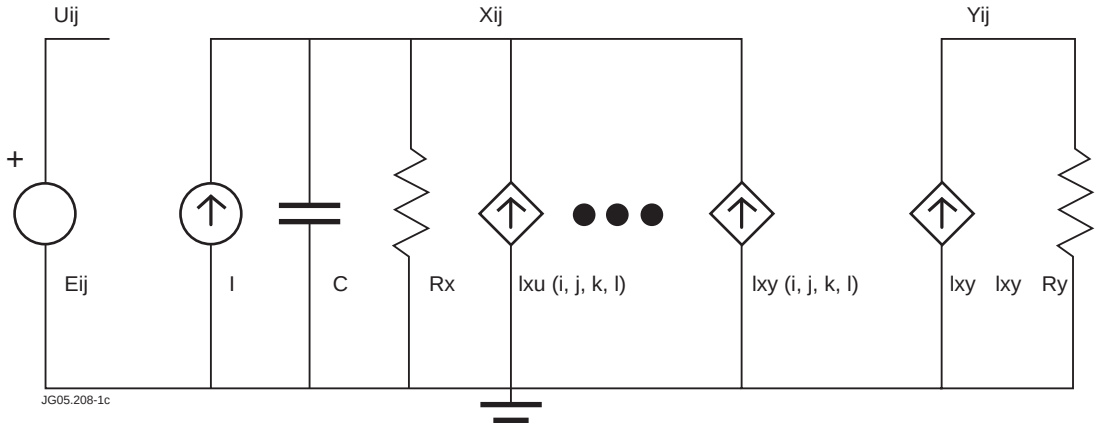

Figure 1: The classical CNN cell scheme.

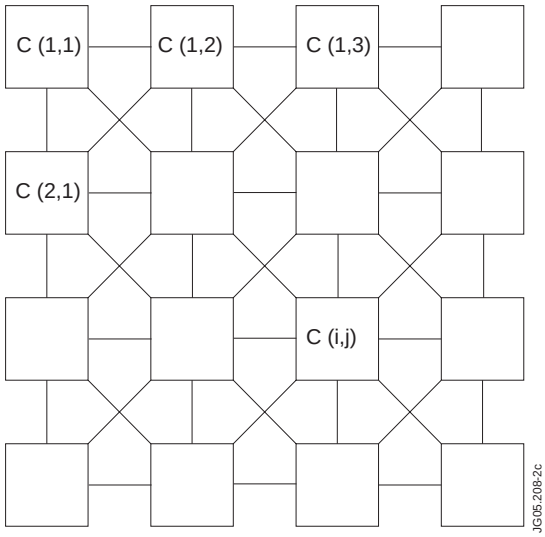

Figure 2: The CNN scheme.

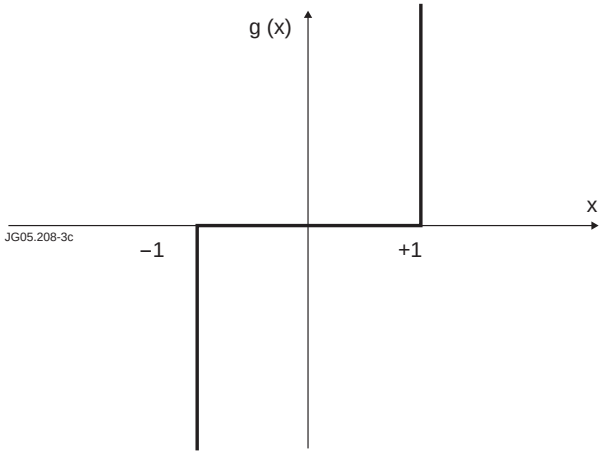

Figure 3: Nonlinear function in the Full Signal Range CNN model, as implemented in the CNN chip.

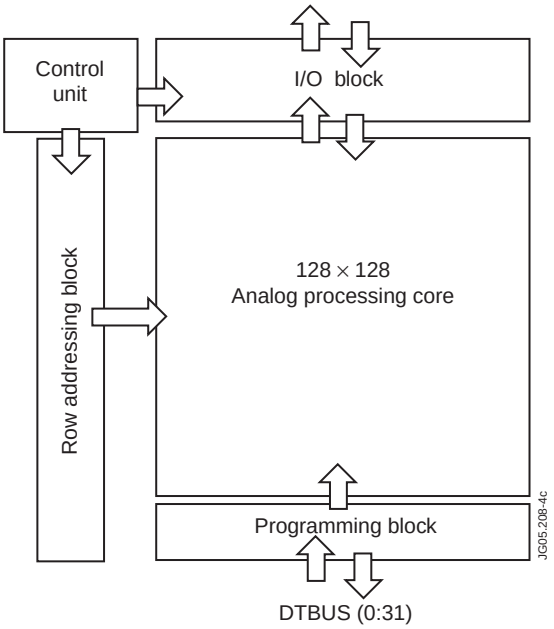

Figure 4: Block Diagram of the ACE16K chip.

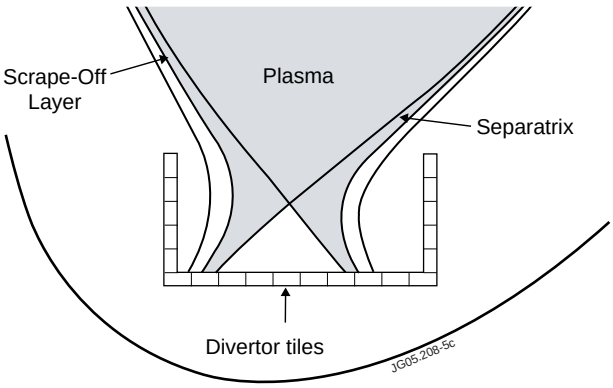

Figure 5: Schematic Outline of JET divertor topology.

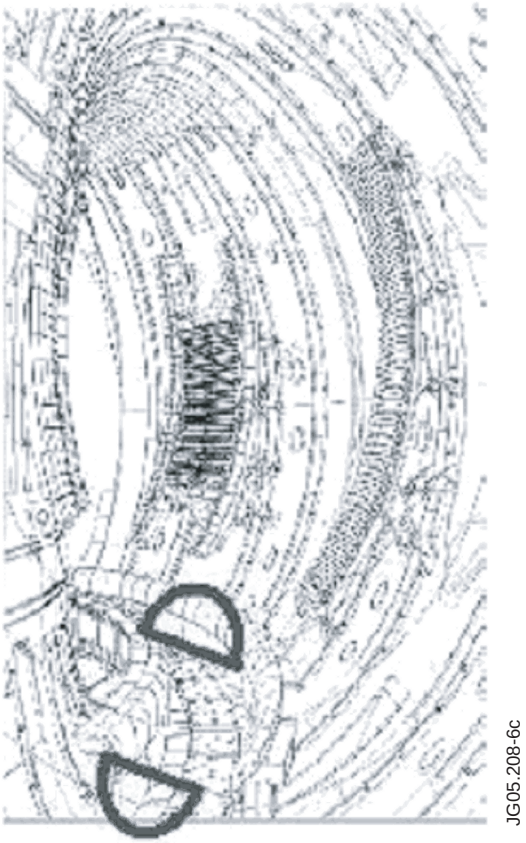

Figure 6: IR views of the divertor.

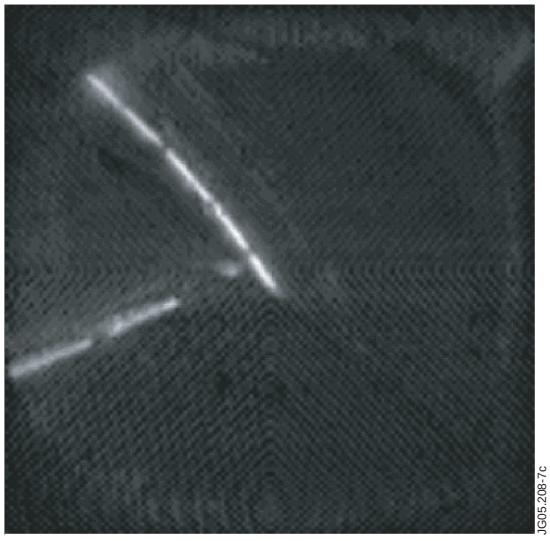

Figure 7: A typical image from the KL3 Infrared Camera.

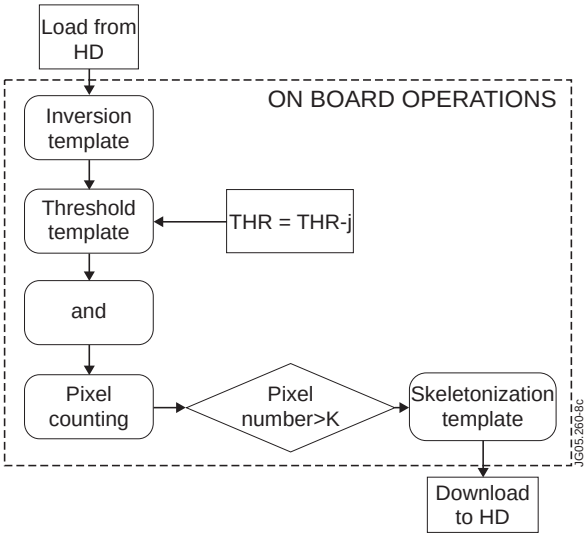

Figure 8: Flow diagram of the implemented algorithm.

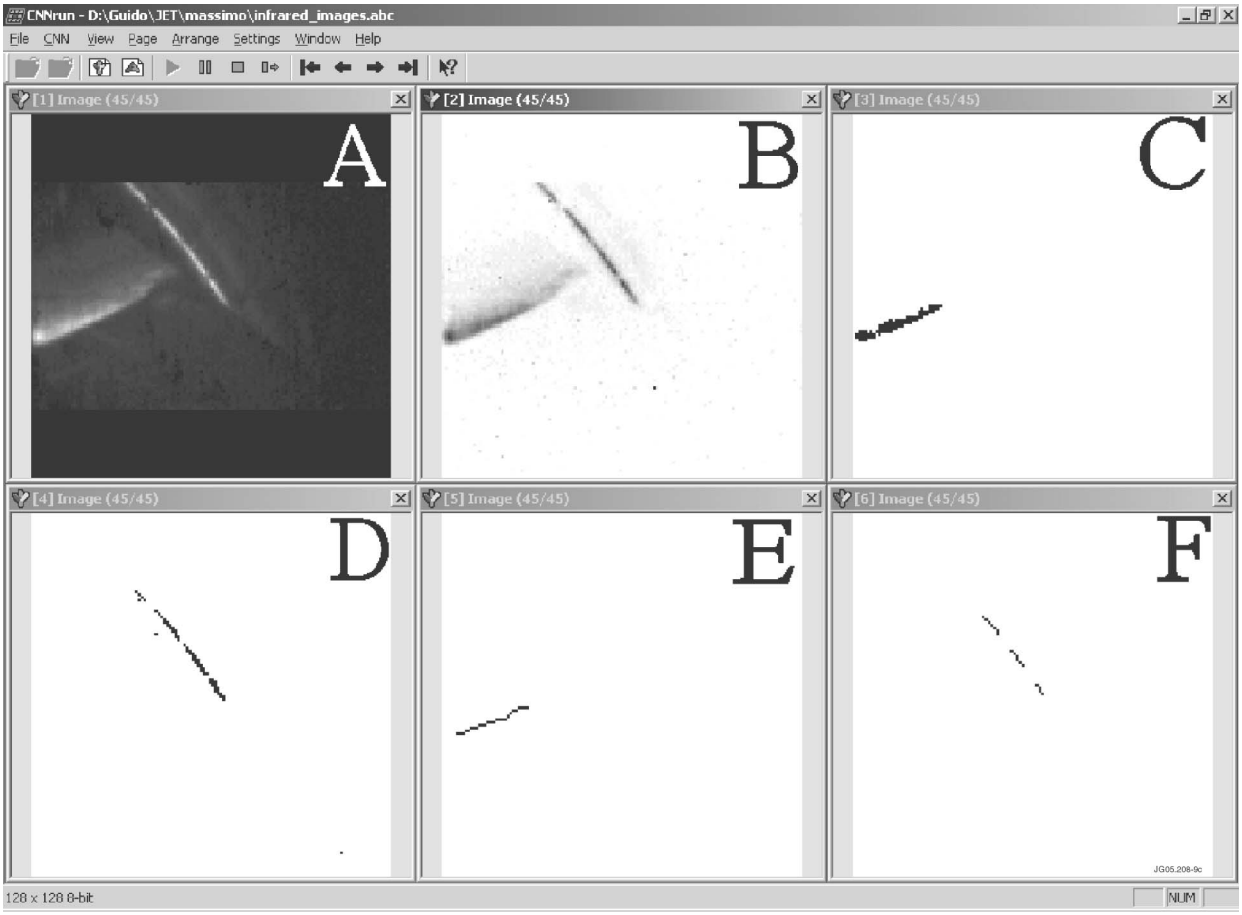

Figure 9: A CNN Run screenshot. Frame A is the starting image, frame B is the result of the inversion template, then C and D are the result of the dynamic threshold for the inner and the outer strike leg respectively, E and F are the final images after the skeletonization template.

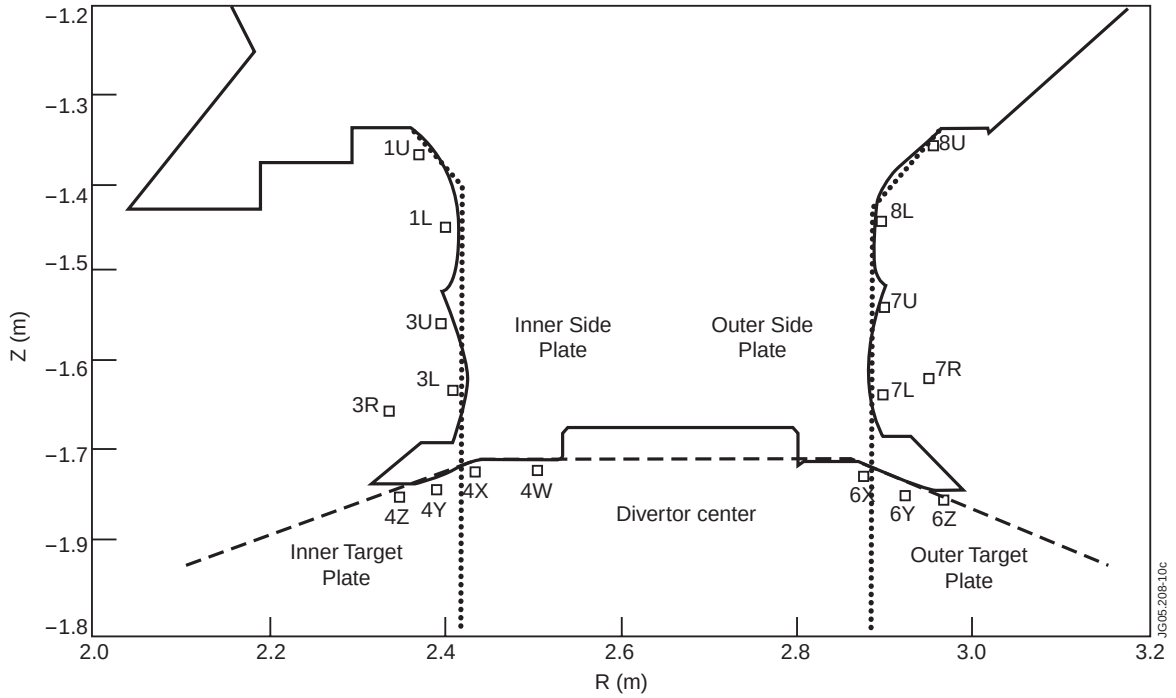

Figure 10: A detailed view of JET divertor section in the poloidal plane. The blue squares represent the thermocouples located in the tiles.

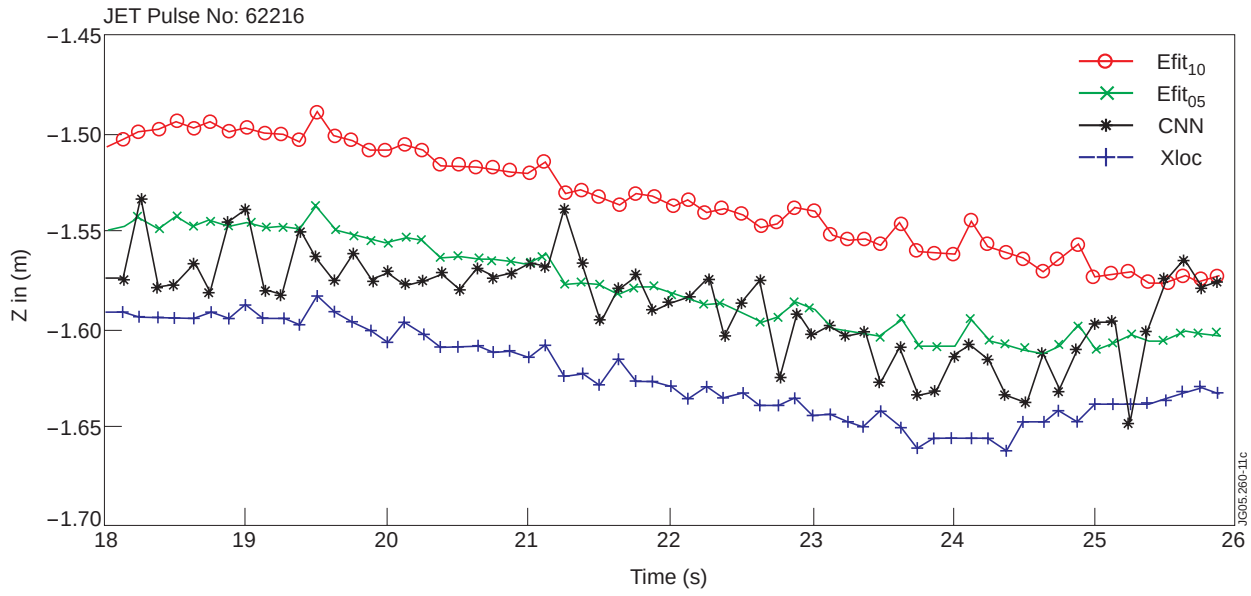

Figure 11: Comparison CNN- Xloc Separatrix and flux expansion line at 5mm and 10mm for the Inner Strike Point (Pulse No: 62216).

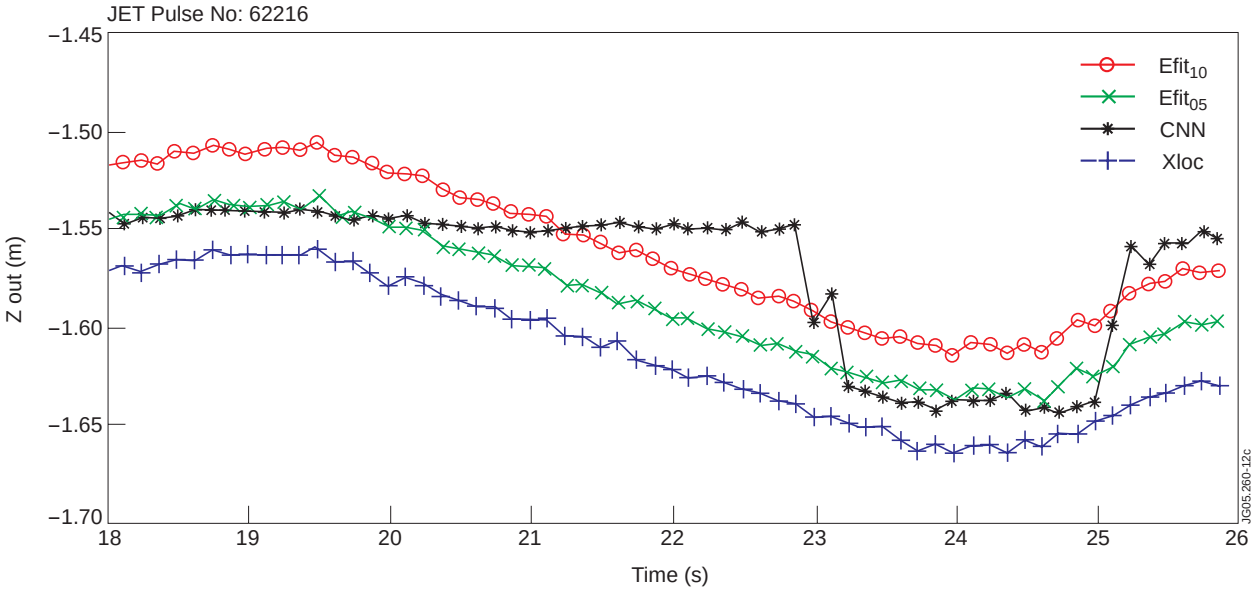

Figure 12: Comparison CNN – Xloc Separatrix and flux expansion line at 5mm and 10mm for the Outer Strike (Pulse No: 62216).

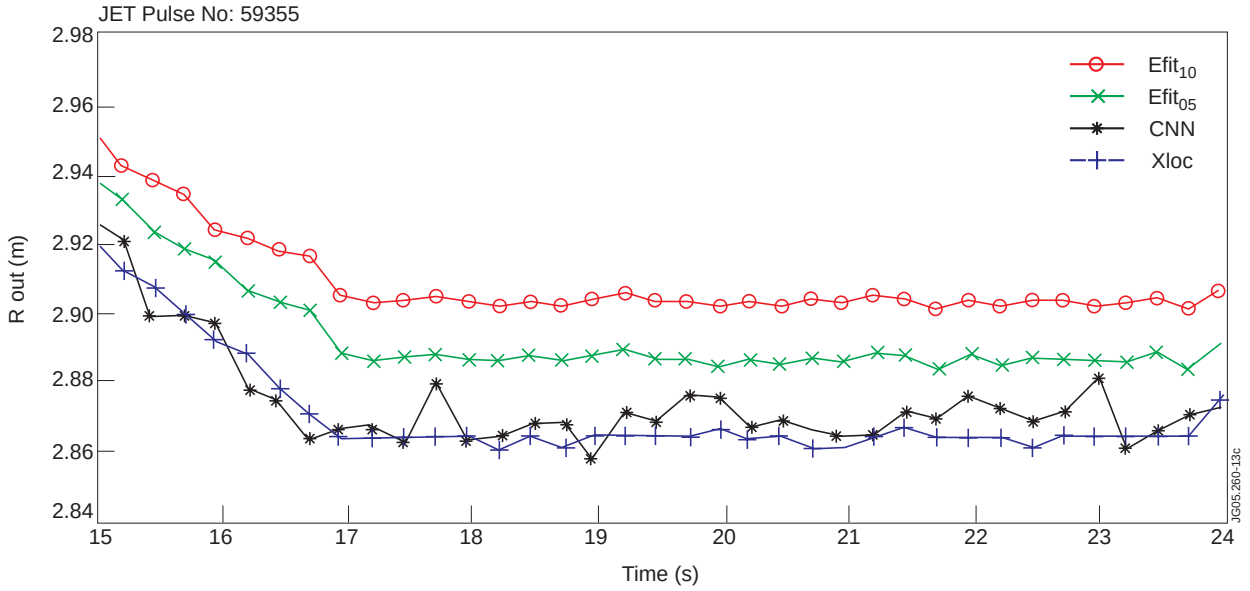

Figure 13: Comparison CNN–Xloc Separatrix and flux expansion line at 5mm and 10mm for the Outer Strike (Pulse No: 59355).

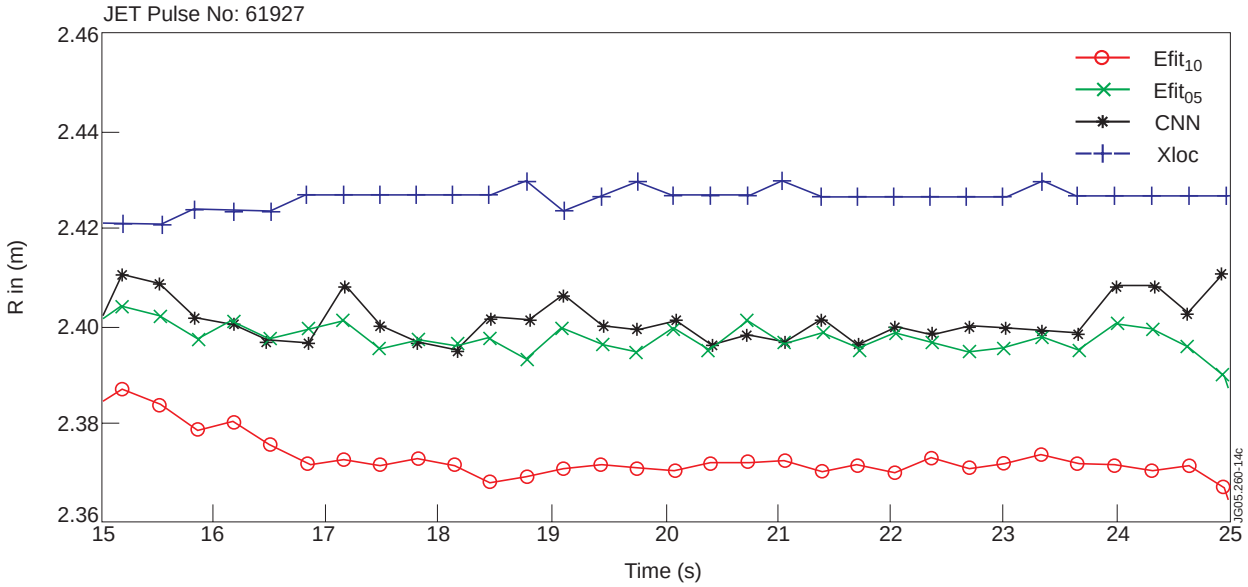

Figure 14: Comparison CNN–Xloc Separatrix and flux expansion line at 5mm and 10mm for the Inner Strike (Pulse No: 61927).

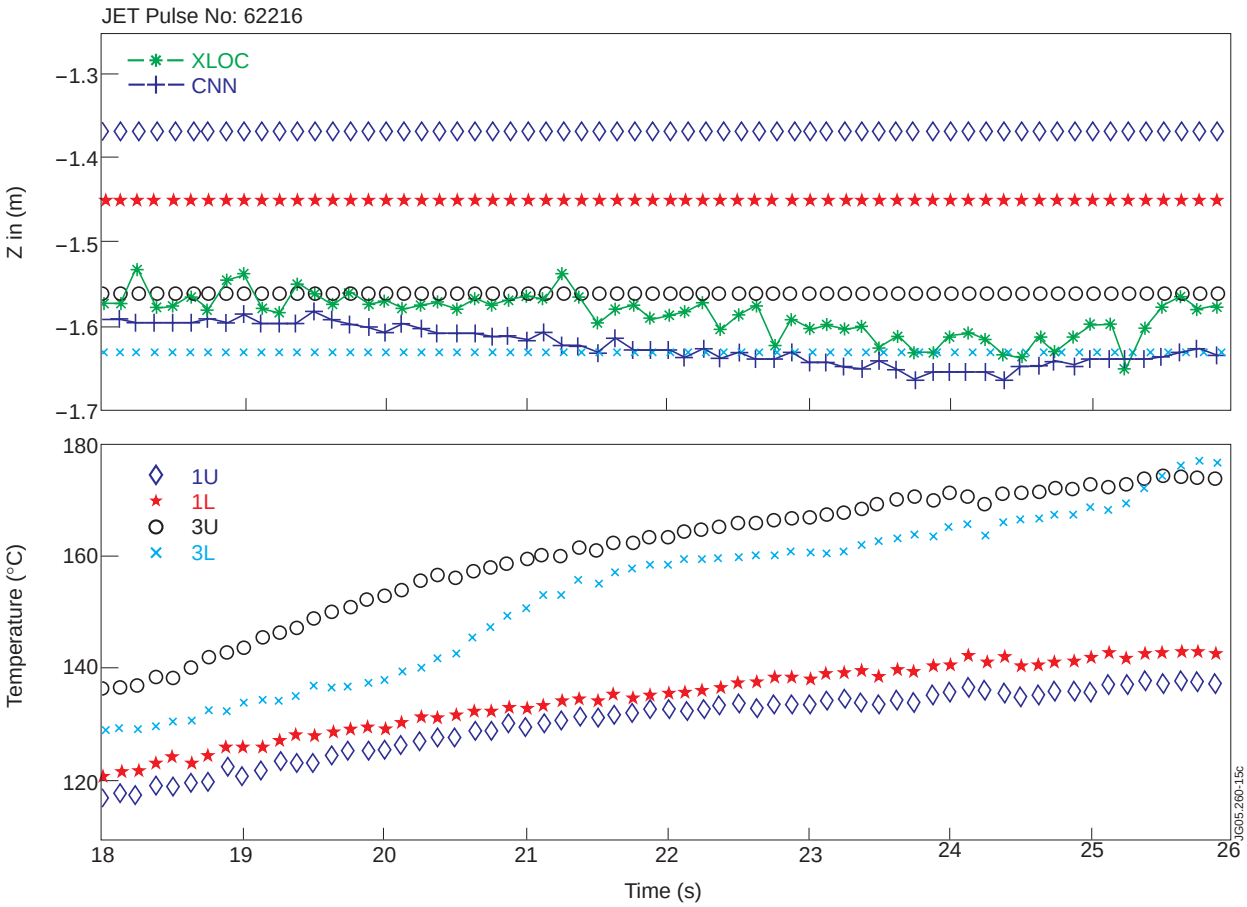

Figure 15: In the top figure the time evolution of the CNN and XLOC calculated strike points is shown, together with the position of the corresponding thermocouple Z in the Inner Side of the divertor. In the bottom figure the time evolution of the thermocouples temperature is shown (Pulse No: 62216).

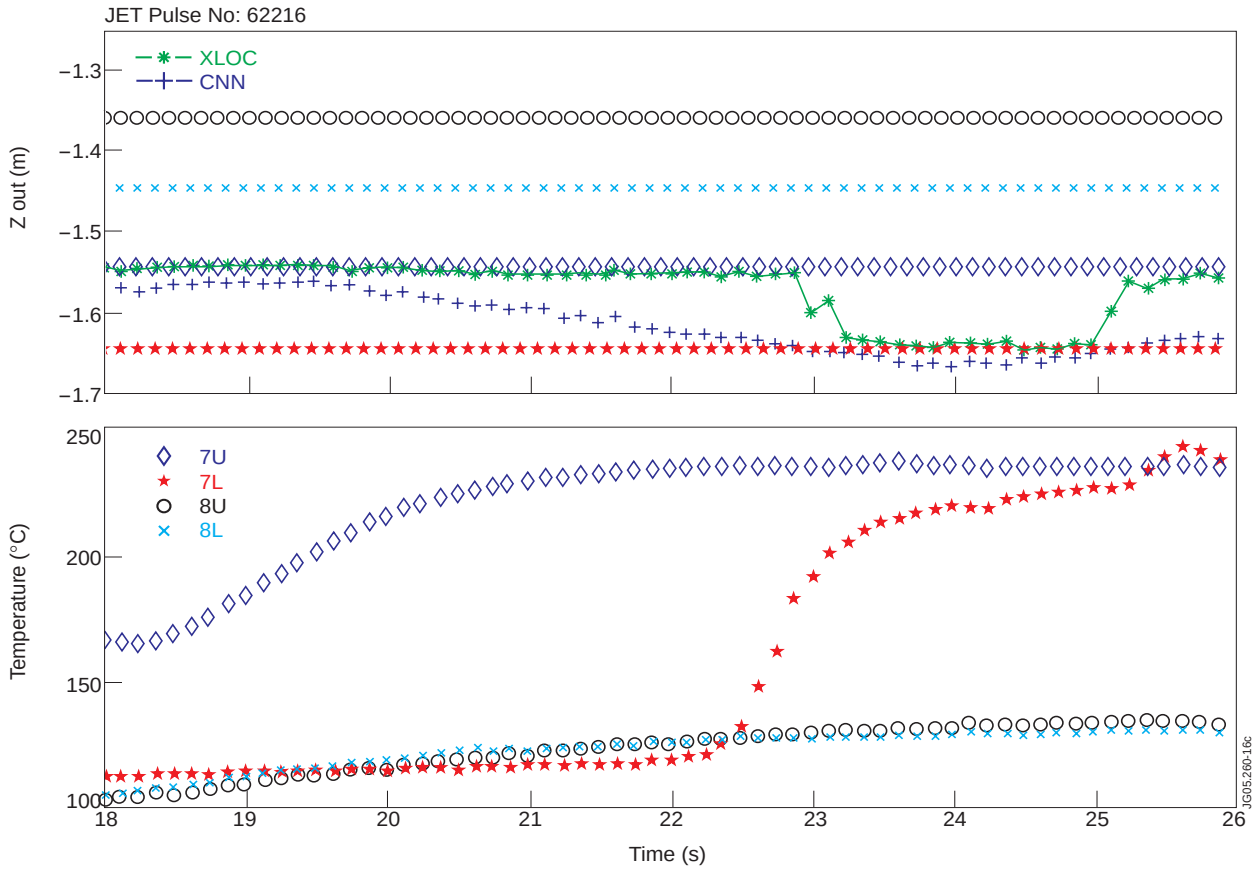

Figure 16: In the top figure the time evolution of the CNN and XLOC calculated strike points is shown, together with the position of the corresponding thermocouple for the coordinate Z in the Outer Side of the divertor. In the bottom figure the time evolution of the thermocouples temperature is shown (Pulse No: 62216).

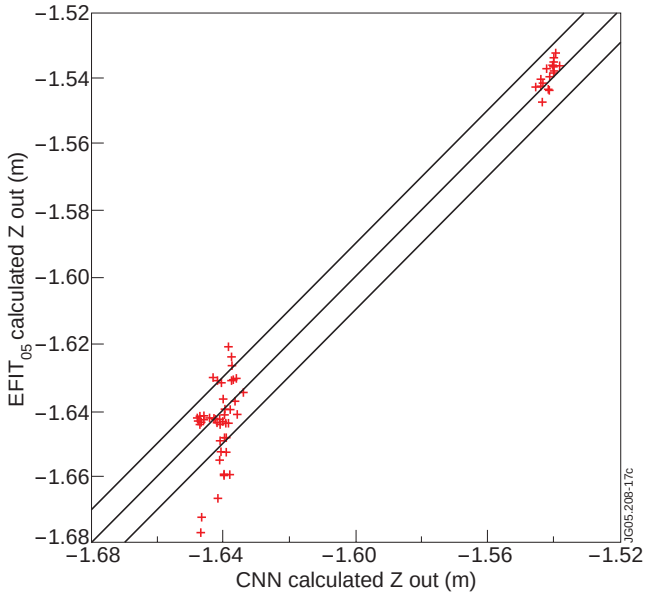

Figure 17: Comparison of the Z estimated of the outer strike point as derived from the CNN and $EFIT_{05}$.